Supplementary Material (ESI) for Chemical Communications
This journal is (c) The Royal Society of Chemistry 2013

Supporting Information

for

Control of Cytochrome *c* Redox Reactivity through Off-Pathway Modifications in Protein Hydrogen-Bonding Network

Jie Gu,[a] Soyeun Yang,[a] Alexander J. Rajic,[b] Igor V. Kurnikov,[c] Tatiana R. Prytkova,[b] and Ekaterina V. Pletneva[a,]*

[a]Department of Chemistry, Dartmouth College, Hanover, NH 03755
[b]Schmid College of Science & Technology, Chapman University, Orange, CA 92866
[c]Department of Chemistry, Carnegie Mellon University, Pittsburgh, PA 15213

Materials and Methods

General. Chemicals were purchased from Fisher Scientific Inc., unless noted otherwise. Buffers were prepared using reagent-grade chemicals. Water was purified to a resistivity of 18 MΩ cm. Data analysis was carried out using MATLAB 2011a (MathWorks).

Mutagenesis, Expression, and Purification of Cyt *c* Mutants. A Cys residue at position 66 in yeast iso-1 cyt *c* was introduced using a Quikchange kit (Agilent) by point mutation of the Rbs(WT*) plasmid, which already contained two background mutations K72A and C102S. The resulting plasmid served as a template for further mutations. DNA was extracted and purified with a QIAprep Spin Miniprep Kit (Qiagen). Mutations were confirmed by sequencing, carried out at the Molecular Biology & Proteomics Core Facility (Dartmouth College). DNA concentrations were determined by the UV absorption measurements. Expression and purification of WT* and mutant proteins were performed

following the published procedures.[1]

Preparation of Ru-labeled Cyt *c* Derivatives. 5-Iodoacetamido-1,10-phenanthroline (phen-IA) and ruthenium (II) bisbipyridine 5-iodoacetamido-1,10-phenanthroline hexafluorophosphate ($[Ru(bpy)_2(IA\text{-}phen)](PF_6)_2$) were synthesized according to the published procedures[2] with the following minor modifications. Iodoacetyl chloride instead of iodoacetic acid was used in the first step of the synthesis. The crude phen-IA product was ground to a powder and washed in a solution of 5% sodium bicarbonate.

The purified protein was pretreated with a ten-fold molar excess of dithiothreitol (DTT) and then applied onto a GE Healthcare HiPrep 26/10 desalting column connected to GE Ätkapurifier FPLC. The column was equilibrated with a 100 mM sodium phosphate buffer at pH 7.7. An approximately five-fold molar excess of $[Ru(bpy)_2(IA\text{-}phen)](PF_6)_2$ over cyt *c* was dissolved in 200 μL of dimethyl sulfoxide and then added to a 100 μM protein solution eluted from the desalting column. The solution mixture was stirred for seven hours at room temperature in the dark. Excess of the labeling reagent was quenched by addition of DTT and the reaction mixture was dialyzed overnight against a 10 mM sodium phosphate buffer at pH 7.4. After dialysis, the protein was oxidized by adding excess of potassium ferricyanide. The ruthenium complex, labeled and unlabeled proteins were separated using a HiTrap SP HP column. Matrix-assisted laser desorption ionization time-of-flight (MALDI-TOF) mass spectrometry measurements confirmed the protein labeling (ABI Voyager-DE Pro MALDI-TOF mass spectrometer, Molecular Biology and Proteomics Core Facility, Dartmouth College).

Spectroscopic Measurements. All samples were diluted to desired concentrations with a 100 mM sodium phosphate buffer at pH 7.4. Absorption spectra were acquired on an Agilent 8453 diode-array and JASCO V-630 scanning spectrophotometers. Circular dichroism (CD) spectra and CD temperature melts were recorded on a JASCO-J815 CD spectropolarimeter equipped with a variable temperature peltier cell device (JASCO, Inc.).

The concentrations of proteins were determined spectrophotometrically with the following extinction coefficients: ε_{410}=106,100 $M^{-1}cm^{-1}$ (ferric) or ε_{416}=129,000 $M^{-1}cm^{-1}$ (ferrous).[3]

Laser Flash Photolysis. Before measurements, samples of Ru-labeled variants were gently deoxygenated with argon gas for 20 min and then thoroughly sealed with a septum. Time-resolved measurements were performed using a Nd:YAG laser (Continuum, Minilite II) generating 5 ns laser pulses at 532 nm as the excitation source and a modified Proteus system (Ultrafast Systems) for detection of transients. Transient absorption was measured with a 75 W Xe lamp (Oriel, model 66912) as the probe source. Both transient absorption and emission were collected perpendicular to the laser pathway with a photodiode (ThorLabs, DET10A) after a monochromator (Spectral Products, model CM110 1/8 m). The signal intensity was digitized using an oscilloscope (Tektronix, DPO 3032). The photolysis system was controlled through the Proteus computer program. For each measurement, at least 512 laser shots were accumulated and averaged.

Protein Structure Models and Molecular Dynamics. The starting point of analysis of the structure and dynamics of cyt *c* mutants was the published crystal structure of C102T ferrous yeast iso-1-cyt c (PDB file: 1YCC).[4] Mutations E66C, K72A, and C(T)102S were introduced and the Ru complex was attached at C66 yielding the model of the first variant Ru^{66}-E66C. Additional mutations N52I and Y67F were introduced to this structure to build models of three other variants. Hydrogen atoms were added by using standard templates of amino acids. All amino acid mutations were made using the HARLEM program.[5] Energy minimization was performed for models of four Ru-labeled proteins to relax close atom-atom contacts that were created upon amino acid modifications. We solvated protein variants by placing them in a box of TIP3P water molecules (55×55×55 $Å^3$). Amber 10 force field was used to describe molecular mechanics models of the solvated proteins.[6]

Harmonic force constants and force constants for valence angles involving metal atoms were set to 100 kcal/mol/$Å^2$ and 63 kcal/mol/rad^2, respectively. These force field

parameters were chosen to maintain local geometries of metal ligands observed in X-ray crystal structures. Periodic boundary conditions and constant pressure conditions were used in molecular dynamics (MD) simulations. For each protein model 100-ns long MD simulations were run. MD snapshots saved each nanosecond during the last 90 ns of MD trajectories were used for calculations of donor-acceptor electronic coupling and ET rates.

Electron Transfer Calculations. Calculations of donor-acceptor electronic coupling H_{AB} were performed using the Green Function method[7, 8] based on Hartree-Fock solution of electronic structure of protein fragments. First we performed *ab initio* Hartree-Fock calculations using 3-21G basis set and Gaussian program.[9] Calculations were done for fragments consisting of donor and acceptor groups as well as bridging protein groups mediating electronic interaction between donor and acceptor. These 'active' fragments were identified using PATHWAYS method with a 5% cutoff criterion.[10] Localized donor-acceptor orbitals (|Di> and |Ai>) were obtained by truncating computed molecular orbitals of the system zeroing LCAO/MO coefficients on all atoms except donor group (for donor localized orbitals) or acceptor group (for acceptor localized orbitals). In the next step we obtained a reduced Hamiltonian in the space of such defined donor-acceptor localized electronic states by computing Green Function $G^{PP}(E)$ (eq 1):

$$G_{kl}^{PP} = \langle k | I \rangle \frac{1}{E - E_I} \langle I | l \rangle \qquad (1)$$

In eq 1, k,l are localized donor and acceptor orbitals, $|I\rangle$ are molecular orbitals and E_I are MO energies. Effective Hamiltonian on localized donor-acceptor states $H_{PP}^{eff}(E)$ was obtained by inversion of Green Function matrix $G^{PP}(E)$ (eq 2):

$$H_{PP}^{eff}(E) = ES_{PP} - S_{PP}G_{PP}(E)^{-1}S_{PP} \qquad (2)$$

In Green Function and effective Hamiltonian calculations, the energy E was taken at -0.2 a.u. around diagonal energies of donor-acceptor states. The effective Hamiltonian matrix

elements on localized donor and acceptor orbitals obtained this way constitute a slow changing function of tunneling energy *E*. Off diagonal elements of this reduced Hamiltonian give values of donor-acceptor electronic couplings H_{DA} that agree well with results obtained with a more involved energy splitting method.[10] ET rate constants k_{ET} were calculated according to eq 3 [10, 11] assuming $-\Delta G^{\circ}=\lambda=1.0$ eV, where $\left\langle H_{DA}^2 \right\rangle$ is the mean square (ensemble-averaged) donor-acceptor electronic coupling:

$$k_{ET} = \left(\frac{4\pi^3}{h^2 \lambda RT} \right)^{1/2} \left\langle H_{DA}^2 \right\rangle exp\left(\frac{-\left(\Delta G^{\circ} + \lambda\right)^2}{4\lambda RT} \right) \quad (3)$$

Ab initio Hartree-Fock (3-21G basis set) calculations were also performed to evaluate interactions ("effective electronic coupling") between the "bridging" molecular orbitals localized on the heme and the aromatic ring of residue 67; see Figure S10 for depiction of these orbitals. According to McConnell,[12] donor-acceptor electronic coupling H_{DA} can be described by eq 4, where V_{DB} and V_{BA} are interactions of orbitals of the bridge with orbitals of the donor and the acceptor, respectively; V_{BB} is the magnitude of the interaction between bridging orbitals; and E_D and E_B are diagonal energies of orbitals of the donor and the bridge, respectively. In the absence of explicit donor and acceptor, the calculated H_{DA} is analogous to V_{BB} and reflects the strength of interactions between the bridging orbitals of the heme and the π system of residue 67.

$$H_{DA} = \frac{V_{DB}}{E_B - E_D} \times \left(\frac{V_{BB}}{E_B - E_D} \right)^{n-1} \times V_{BA} \quad (4)$$

Supplementary Material (ESI) for Chemical Communications
This journal is (c) The Royal Society of Chemistry 2013

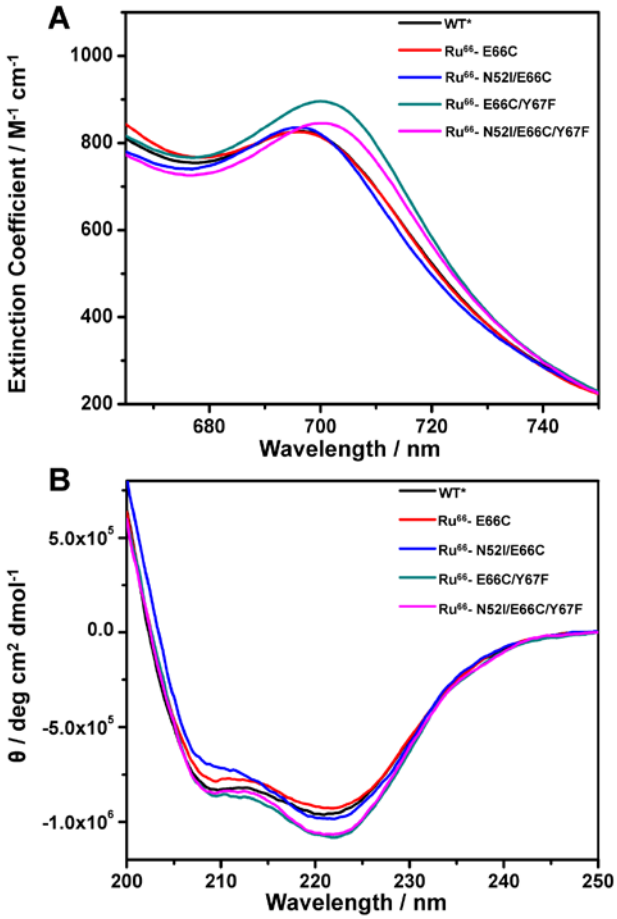

Figure S1. (A) Near-IR absorption and (B) far-UV CD spectra of ferric WT* (*black*) and Ru-labeled cyt *c* variants (Ru^{66}-E66C, *red*; Ru^{66}-N52I/E66C, *blue*; Ru^{66}-E66C/Y67F, *green*; Ru^{66}-N52I/E66C/Y67F, *magenta*) in a 100 mM sodium phosphate buffer at pH 7.4.

Supplementary Material (ESI) for Chemical Communications
This journal is (c) The Royal Society of Chemistry 2013

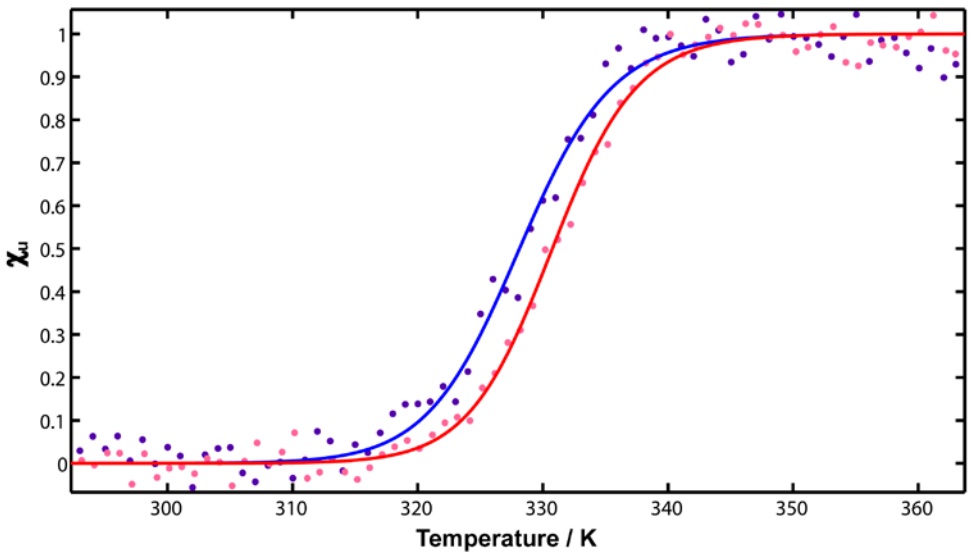

Figure S2. CD melting curves (monitored at 222 nm) for ferric WT* (*red*) and Ru^{66}-E66C (*blue*) iso-1 cyt *c* in a 100 mM sodium phosphate buffer at pH 7.4.

Supplementary Material (ESI) for Chemical Communications
This journal is (c) The Royal Society of Chemistry 2013

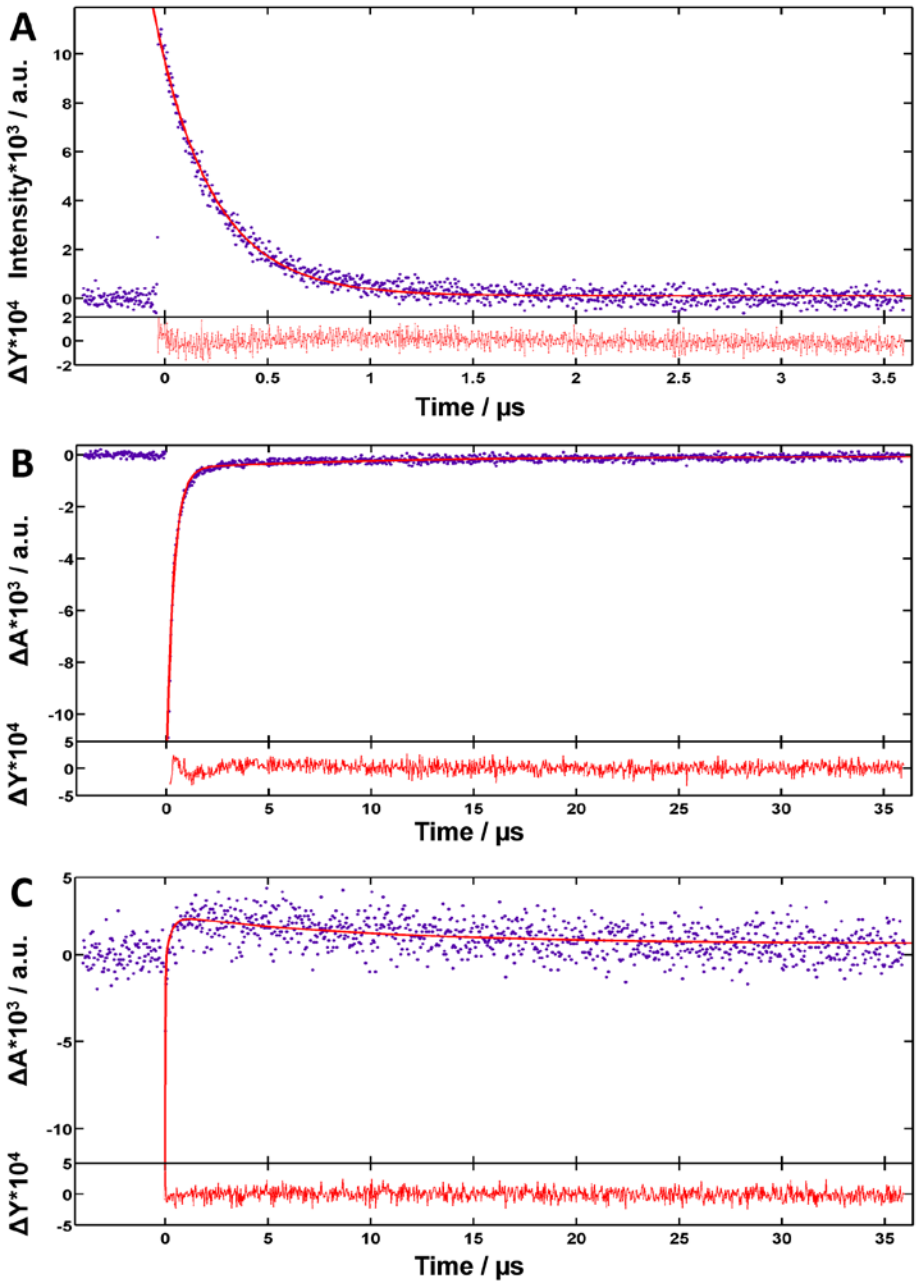

Figure S3. (A) Emission at 630 nm and transient absorption traces at (B) 450 nm and (C) 550 nm of Ru^{66}-E66C after laser flash excitation. The emission decay is monoexponential, while the two transient absorption traces require fits to biexponential functions. The rate constants from fits (*red* lines) are $k_1 + k_d = 3.4 \pm 0.3\ \mu s^{-1}$, $k_2 = 0.12 \pm 0.01\ \mu s^{-1}$; fit residuals for each trace are shown in corresponding lower panels.

Supplementary Material (ESI) for Chemical Communications
This journal is (c) The Royal Society of Chemistry 2013

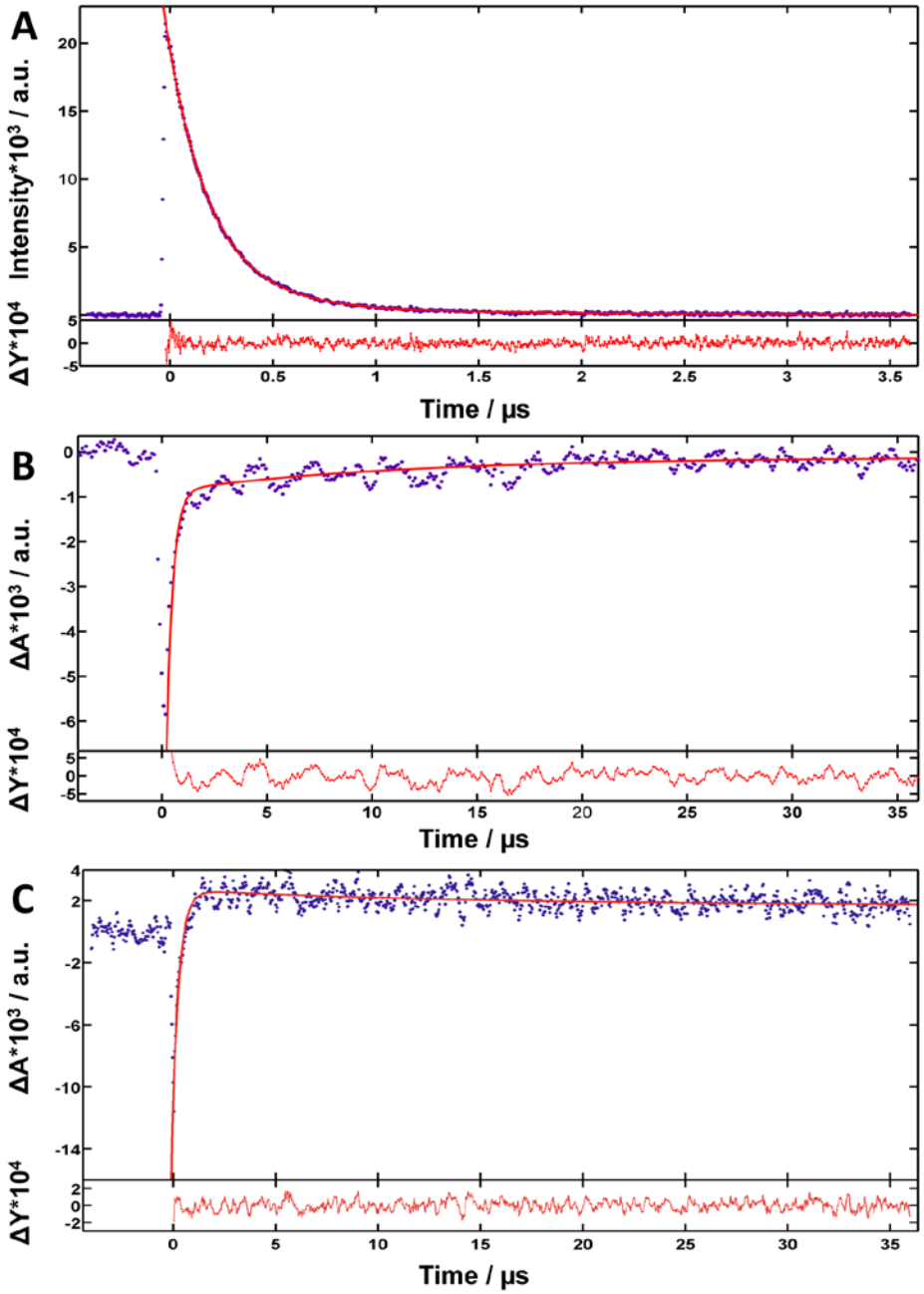

Figure S4. (A) Emission at 630 nm and transient absorption traces at (B) 450 nm and (C) 550 nm of Ru^{66}-N52I/E66C after laser flash excitation. The emission decay is monoexponential, while the two transient absorption traces require fits to biexponential functions. The rate constants from fits (*red* lines) are $k_1 + k_d = 3.0 \pm 0.2\ \mu s^{-1}$, $k_2 = 0.10 \pm 0.01\ \mu s^{-1}$; fit residuals for each trace are shown in corresponding lower panels.

Supplementary Material (ESI) for Chemical Communications
This journal is (c) The Royal Society of Chemistry 2013

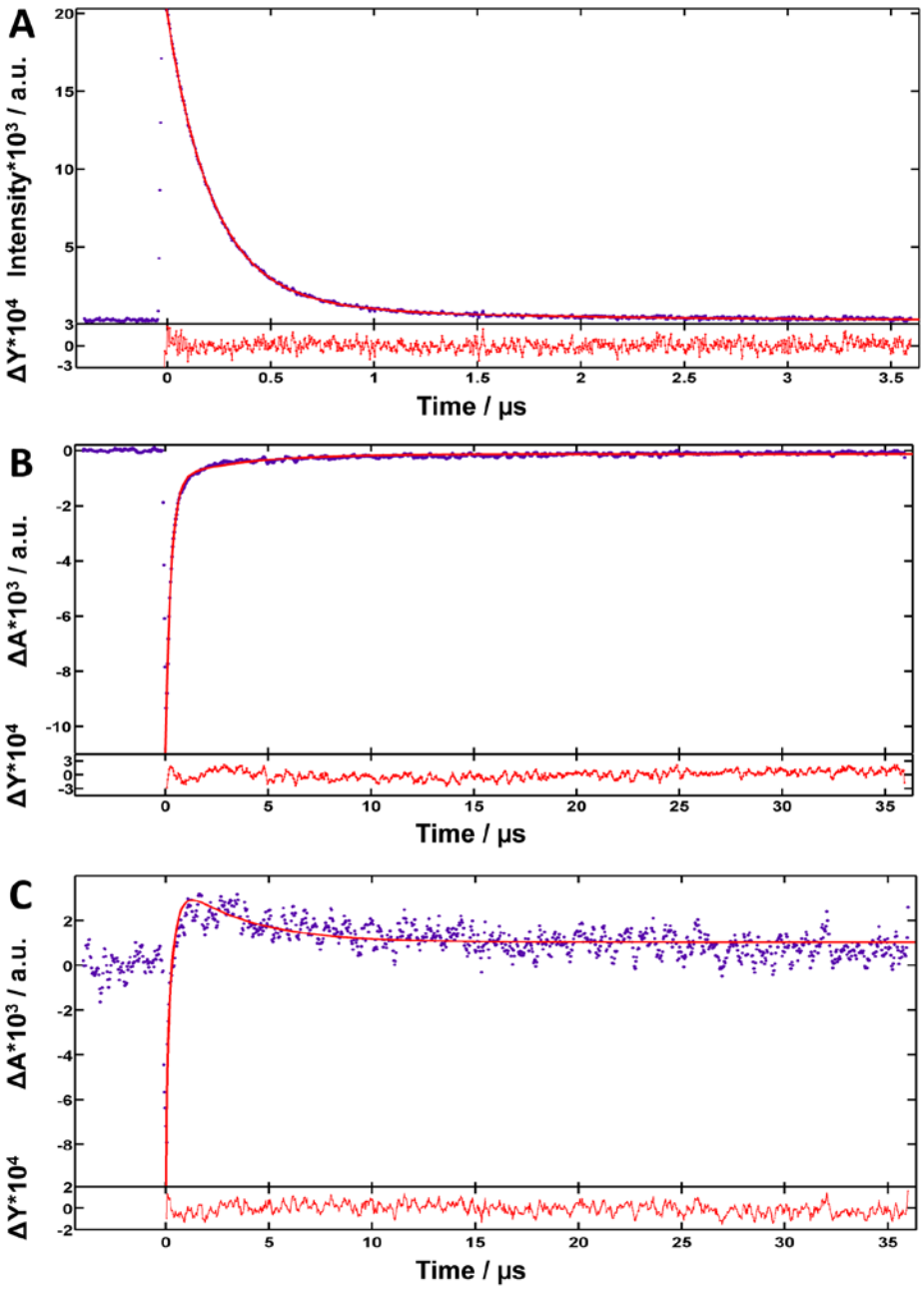

Figure S5. (A) Emission at 630 nm and transient absorption traces at (B) 450 nm and (C) 550 nm of Ru^{66}-E66C/Y67F after laser flash excitation. The emission decay is monoexponential, while the two transient absorption traces require fits to biexponential functions. The rate constants from fits (*red* lines) are $k_1 + k_d = 3.7 \pm 0.1\ \mu s^{-1}$, $k_2 = 0.38 \pm 0.08\ \mu s^{-1}$; fit residuals for each trace are shown in corresponding lower panels.

Supplementary Material (ESI) for Chemical Communications
This journal is (c) The Royal Society of Chemistry 2013

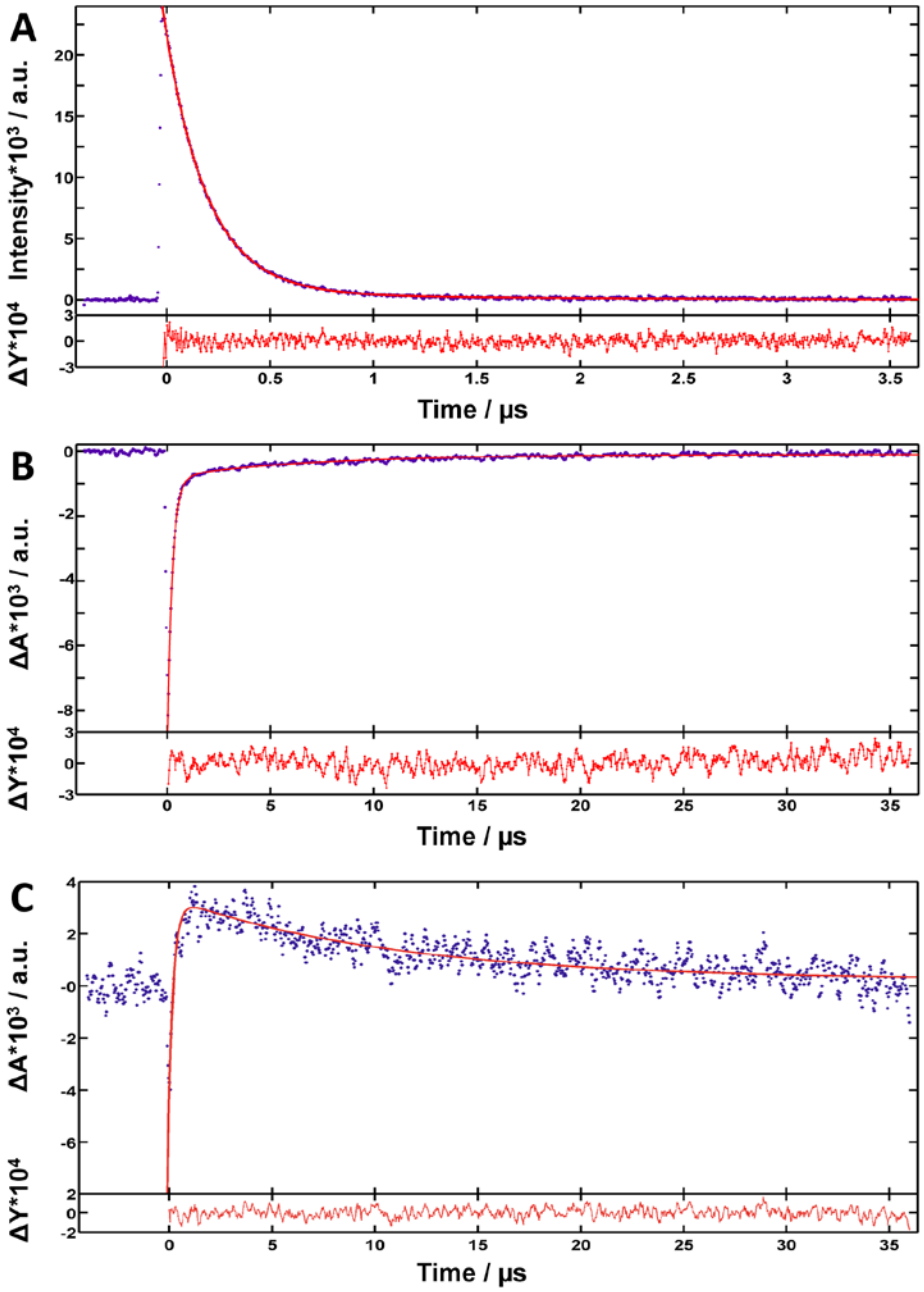

Figure S6. (A) Emission at 630 nm and transient absorption traces at (B) 450 nm and (C) 550 nm of Ru^{66}-N52I/E66C/Y67F after laser flash excitation. The emission decay is monoexponential, while the two transient absorption traces require fits to biexponential functions. The rate constants from fits (*red* lines) are $k_1 + k_d = 4.0 \pm 0.4\ \mu s^{-1}$, $k_2 = 0.12 \pm 0.01\ \mu s^{-1}$; fit residuals for each trace are shown in corresponding lower panels.

Supplementary Material (ESI) for Chemical Communications
This journal is (c) The Royal Society of Chemistry 2013

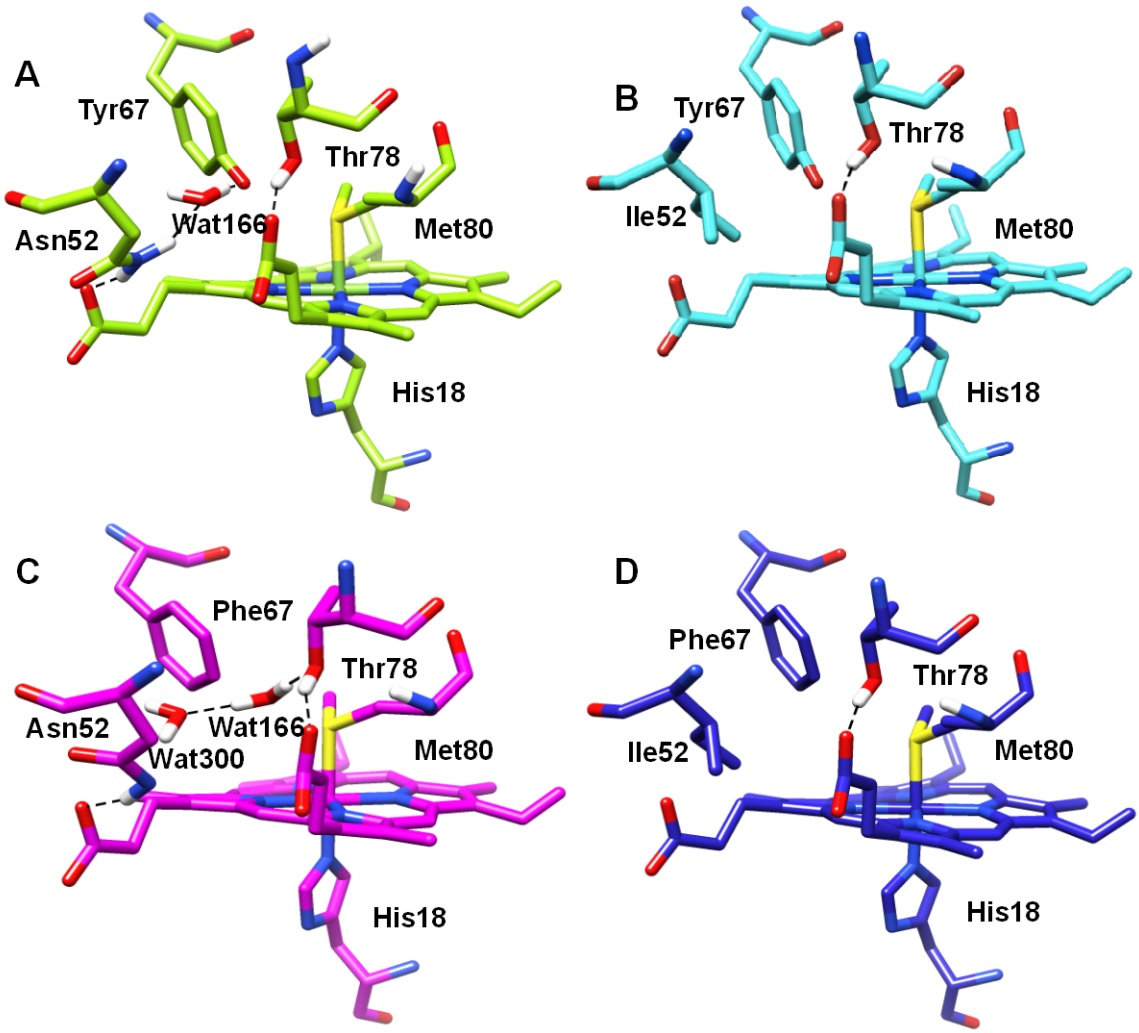

Figure S7. Heme, heme ligands, residues 52 and 67, as well as Thr78 and internal water molecules in (A) Ru^{66}-E66C (*green*), (B) Ru^{66}-N52I/E66C (*cyan*), (C) Ru^{66}-E66C/Y67F (*pink*), and (D) Ru^{66}-N52I/E66C/Y67F (*blue*) variants of cyt *c*. In each case, hydrogen bonds are shown as black dash lines. Oxygen atoms are shown in *red*, nitrogen atoms in *blue*, and sulfur atoms in *yellow*. Shown are average structures from MD simulations.

Supplementary Material (ESI) for Chemical Communications
This journal is (c) The Royal Society of Chemistry 2013

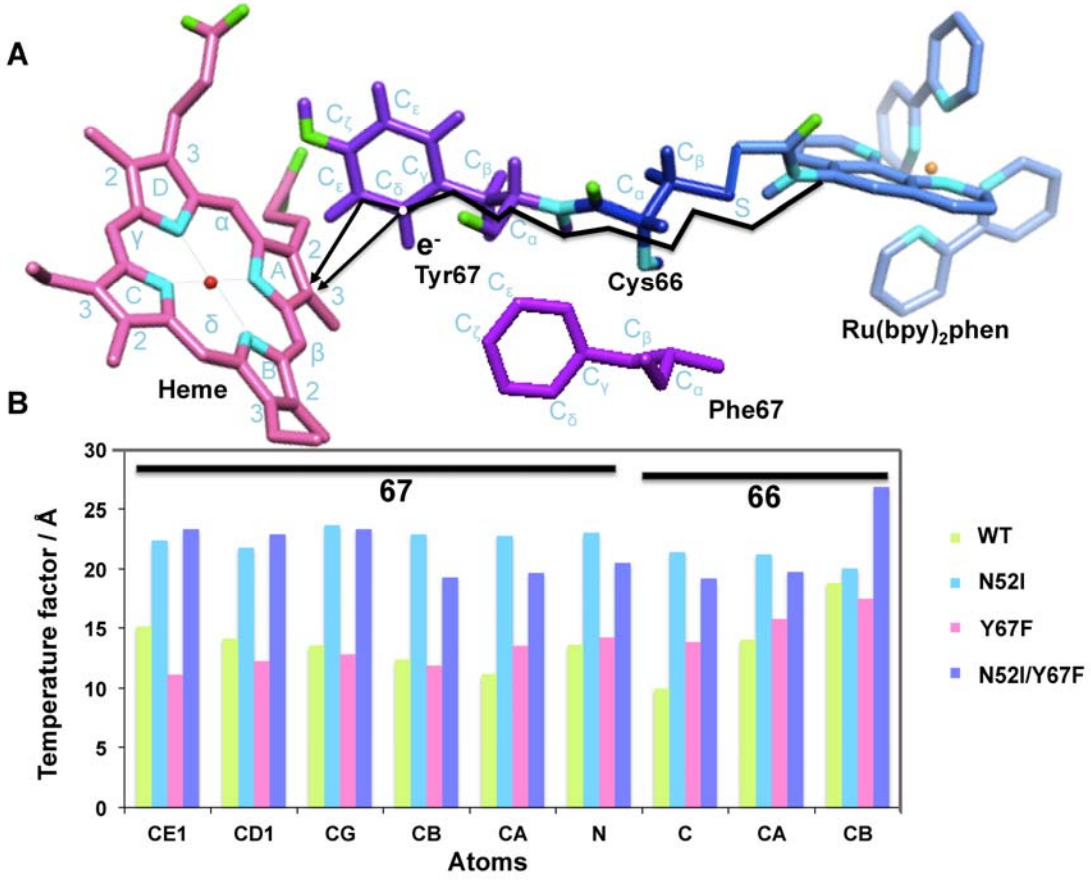

Figure S8. (A) The protein fragment along the two dominant ET pathways. (B) Temperature factors of atoms along these pathways from crystal structures of variants in their ferrous states (PDB files: WT, 1YCC; N52I, 1CRH; Y67F, 1CTZ; N52I/Y67F, 1CRJ).

Supplementary Material (ESI) for Chemical Communications
This journal is (c) The Royal Society of Chemistry 2013

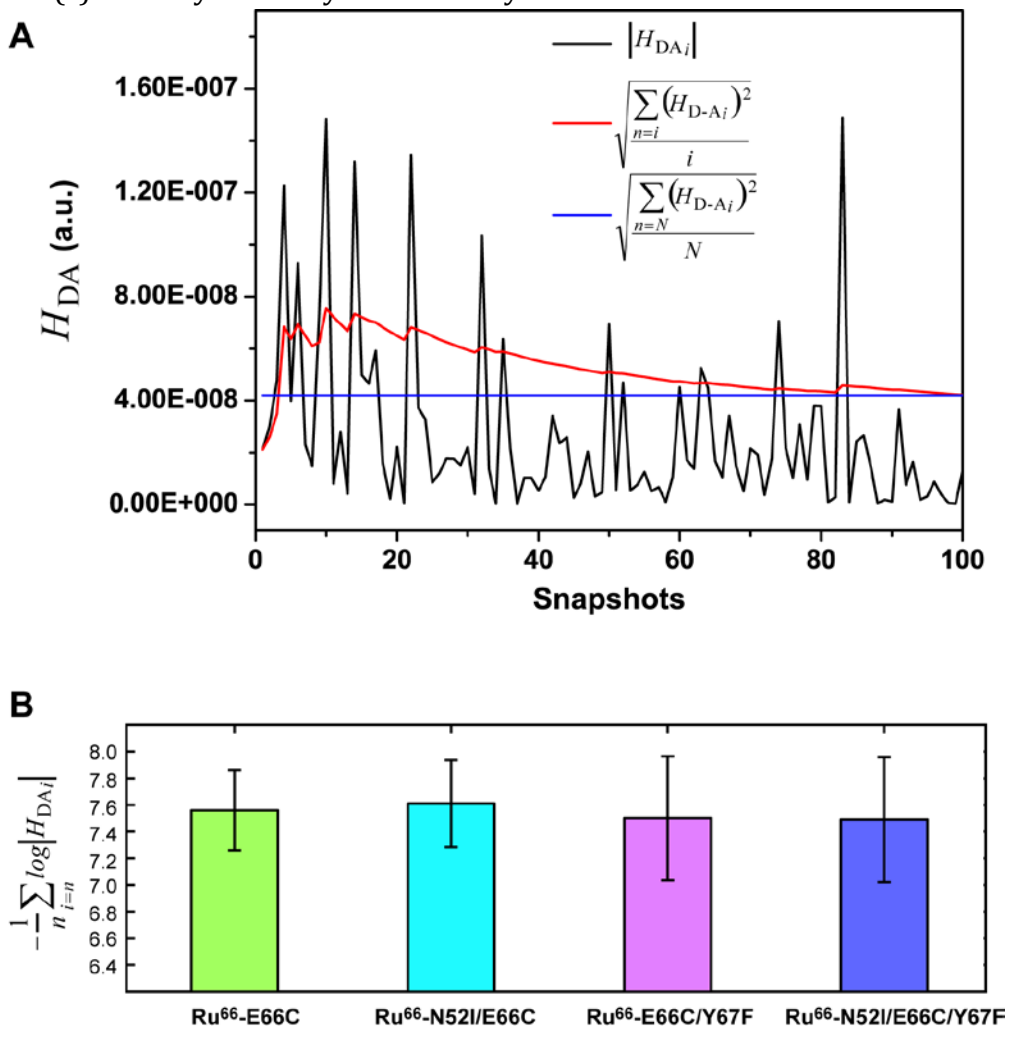

Figure S9. (A) Absolute values of calculated electronic couplings $|H_{DA_i}|$ (*black*) for different structures (snapshots sampled every 1 ns) from 100-ns long MD simulations of Ru^{66}-E66C; running root mean square $\langle H_{DA}^2 \rangle^{1/2}$ (*red*, *n*=*i*, *i* is the number of snapshots averaged); and root mean square $\langle H_{DA}^2 \rangle^{1/2}$ for the complete set (*blue*, *n*=*N*=100). Already at 50 ns the *blue* and *red* lines start to converge, extending MD simulations to 100 ns further improves the convergence. (B) Calculated values of $-\frac{1}{n}\sum_{i=n} log|H_{DA_i}|$ for four variants and their root-mean-square deviations (displayed as error bars). The average couplings are very similar but the individual values fluctuate more for the two variants having Y67F mutation. Fluctuations in electronic couplings reflect fluctuations in protein structure and are consistent with the data in Figure 2C in the main text.

Supplementary Material (ESI) for Chemical Communications
This journal is (c) The Royal Society of Chemistry 2013

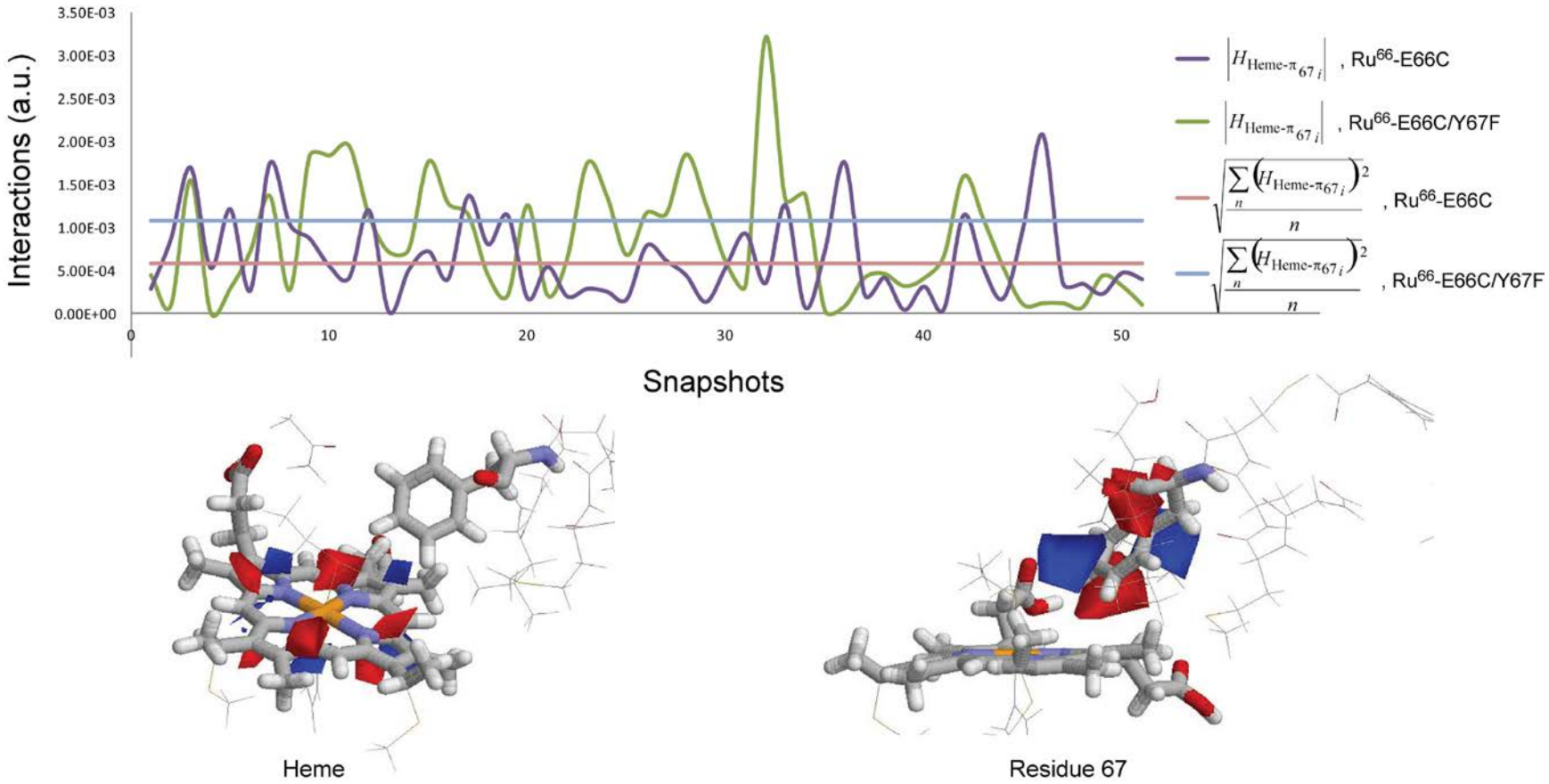

Figure S10. Interactions ("effective electronic coupling") between molecular orbitals localized on the heme and the aromatic ring of residue 67. The value of these interactions depends strongly on protein conformation (notice fluctuations in this parameter from different MD snapshots), but the root-mean-square value $\left\langle H_{\text{DA}}^2 \right\rangle^{1/2}$ (averaged over all snapshots) is larger for the Ru^{66}-E66C/Y67F variant compared to that for the Ru^{66}-E66C variant. The enhancement of these interactions (owing to sampling of different protein conformations) for the Ru^{66}-E66C/Y67F variant largely accounts the increased overall Ru-Fe electronic coupling $\left\langle H_{\text{DA}}^2 \right\rangle^{1/2}$ and faster ET rates in the Ru^{66}-E66C/Y67F variant.

Supplementary Material (ESI) for Chemical Communications
This journal is (c) The Royal Society of Chemistry 2013

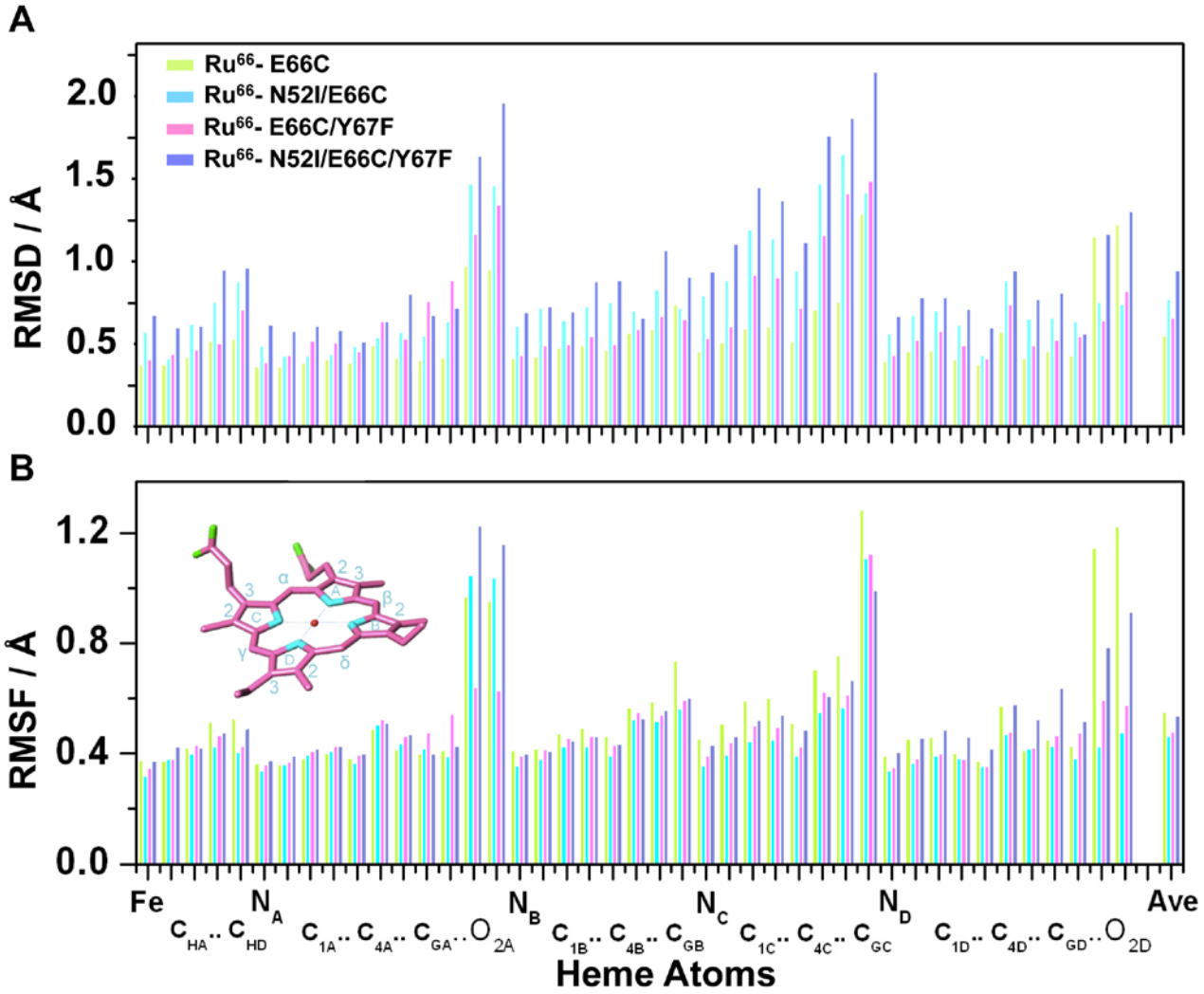

Figure S11. (A) Root-Mean-Square Deviation (RMSD) and (B) Root-Mean-Square Fluctuations (RMSF) of all the atoms (except hydrogens) of the heme group of Ru^{66}-E66C (*green*), Ru^{66}-N52I/E66C (*cyan*), Ru^{66}-E66C/Y67F (*pink*), and Ru^{66}-N52I/E66C/Y67F (*blue*) from MD simulations.

Table S1. Thermodynamic Parameters from Thermal Denaturation of WT (WT*) and Ru-labeled Variants of Yeast Iso-1 Cyt *c*[a]

Variant	WT (WT*)	N52I	Y67F	N52I/Y67F
		ferric		
T_m (°C)	53.6 ± 0.3[b] (59.4 ± 0.5)[c]	66.1 ± 0.2[b]	58.3 ± 0.2[b]	70.9 ± 0.2[b]
ΔH_m (kJ mol^{-1})	418 ± 4[b] (366 ± 8)[c]	514[b]	464[b]	556[b]
		With E66C Mutation and Ru^{66} Labeling[c]		
T_m (°C)	55.7 ± 0.7	62.5 ± 0.3	57.1 ± 0.6	67.5 ± 0.3
ΔH_m (kJ mol^{-1})	189 ± 20	355 ± 33	300 ± 40	377 ± 40
		ferrous		
T_m (°C)	80.3 ± 0.3[b] (85.9 ± 0.6)[c]	87.2 ± 0.2[b]	81.1 ± 0.2[b]	91.2 ± 0.2[b]
ΔH_m (kJ mol^{-1})	577 ± 8[b] (544 ± 8)[c]	623[b]	585[b]	673[b]
		With E66C Mutation and Ru^{66} Labeling[c]		
T_m (°C)	82.6 ± 0.6	87.8 ± 4.0	84.6 ± 1.6	91.8 ± 7.7
ΔH_m (kJ mol^{-1})	478 ± 70	306 ± 85	492 ± 95	550 ± 382

[a]WT is the protein expressed in yeast with trimethylated K72 and C102T mutation; WT* is the protein expressed in *E. coli* with mutations K72A and C102S. [b]Literature values; determined with DSC measurements in a 50 mM sodium acetate buffer at pH 4.7.[13] The protein has trimethylated K72 and additional mutation C102T (from the WT background). [c]Experimental values in a 100 mM sodium phosphate buffer at pH 7.4 from this work; determined with CD measurements at 222 nm. The protein has additional mutations K72A and C102S (from the WT* background) and E66C mutation for Ru labeling.

Supplementary Material (ESI) for Chemical Communications
This journal is (c) The Royal Society of Chemistry 2013

Table S2. Position of Residue 67 in Yeast Iso-1 Ferrocyt *c*

Variant	Ru^{66}(E66C)	Ru^{66}(N52I/E66C)	Ru^{66}(Y67F/E66C)	Ru^{66}(N52I/Y67F/E66C)
			Crystal Structure[a]	
Space jump length (residue 67 CD1 - heme C3A) (Å)	4.473	4.169	4.573	4.440
Space jump length (residue 67 CE1 - heme C3A) (Å)	3.640	3.578	3.707	3.599
Torsional Angle residue 67.CG CZ - heme.Fe NA (°)	-80.697	-76.030	-79.153	-78.299
			MD Simulations[b]	
Space jump length (residue 67 CD1 - heme C3A) (Å)	4.322	4.358	4.736	4.472
Space jump length (residue 67 CE1 - heme C3A) (Å)	3.801	3.787	3.731	3.869
Torsional Angle residue 67.CG CZ - heme.Fe NA (°)	-72.257	-79.613	-95.254	-79.870

[a]Unlabeled variants that contain the native E66 residue, trimethylated K72, and the background C102T mutation; PDB files: WT, 1YCC; N52I, 1CRH; Y67F, 1CTZ; N52I/Y67F, 1CRJ. [b]Model structures have background mutations K72A and C102S (as in our kinetic experiments) and Ru complex, parameters from analyses of average structures are shown.

Supplementary Material (ESI) for Chemical Communications
This journal is (c) The Royal Society of Chemistry 2013

References

1. J. Hanske, J. R. Toffey, A. M. Morenz, A. J. Bonilla, K. H. Schiavoni and E. V. Pletneva, *Proc Natl Acad Sci U S A*, 2012, **109**, 125-130.

2. F. N. Castellano, J. D. Dattelbaum and J. R. Lakowicz, *Anal Biochem*, 1998, **255**, 165-170.

3. A. L. Raphael, D. Wuttke and H. B. Gray, *Biochemistry*, 1990, **29**, 2204-2204.

4. G. V. Louie and G. D. Brayer, *J Mol Biol*, 1990, **214**, 527-555.

5. I. V. Kurnikov, HARLEM molecular modeling package, Department of Chemistry, University of Pittsburgh, Pittsburgh, PA, 2000.

6. D. A. Case, T. A. Darden, T. E. Cheatham, III, C. L. Simmerling, J. Wang, R. E. Duke, R. Luo, M. Crowley, R. C.Walker,W. Zhang, K. M. Merz, B. Wang, S. Hayik, A. Roitberg, G. Seabra, I. Kolossváry, K. F.Wong, F. Paesani, J. Vanicek, X. Wu, S. R. Brozell, T. Steinbrecher, H. Gohlke, L. Yang, C. Tan, J. Mongan, V. Hornak, G. Cui, D. H. Mathews, M. G. Seetin, C. Sagui, V. Babin, and P. A. Kollman (2008), AMBER 10, University of California, San Francisco.

7. I. V. Kurnikov and D. N. Beratan, *J Chem Phys*, 1996, **105**, 9561.

8. M. R. Hartings, I. V. Kurnikov, A. R. Dunn, J. R. Winkler, H. B. Gray and M. A. Ratner, *Coord Chem Rev*, 2010, **254**, 248-253.

9. M. J. Frisch, G. W. Trucks, H. B. Schlegel, G. E. Scuseria, M. A. Robb, J. R. Cheeseman, G. Scalmani, V. Barone, B. Mennucci, G. A. Petersson, H. Nakatsuji, M. Caricato, X. Li, H. P. Hratchian, A. F. Izmaylov, J. Bloino, G. Zheng, J. L. Sonnenberg, M. Hada, M. Ehara, K. Toyota, R. Fukuda, J. Hasegawa, M. Ishida, T. Nakajima, Y. Honda, O. Kitao, H. Nakai, T. Vreven, J. A. Montgomery, J. E. Peralta, F. Ogliaro, M. Bearpark, J. J. Heyd, E. Brothers, K. N. Kudin, V. N. Staroverov, R. Kobayashi, J. Normand, K. Raghavachari, A. Rendell, J. C. Burant, S. S. Iyengar, J. Tomasi, M. Cossi, N. Rega, J. M. Millam, M. Klene, J. E. Knox, J. B. Cross, V. Bakken, C. Adamo, J. Jaramillo, R. Gomperts, R. E. Stratmann, O. Yazyev, A. J. Austin, R. Cammi, C. Pomelli, J. W. Ochterski, R. L. Martin, K. Morokuma, V. G. Zakrzewski, G. A. Voth, P. Salvador, J. J. Dannenberg, S. Dapprich, A. D. Daniels, Farkas, J. B. Foresman, J. V. Ortiz, J. Cioslowski and D. J. Fox, , Gaussian 09, (Revision D.01), Wallingford CT, 2009.

10. T. R. Prytkova, I. V. Kurnikov and D. N. Beratan, *J Phys Chem B*, 2005, **109**, 1618-1625.

11. R. A. Marcus and N. Sutin, *Biochim Biophys Acta*, 1985, **811**, 265-322.

12. H. M. McConnell, *J Chem Phys*, 1961, **35**, 508-515.

13. C. M. Lett, A. M. Berghuis, H. E. Frey, J. R. Lepock and J. G. Guillemette, *J Biol Chem*, 1996, **271**, 29088-29093.